

See discussions, stats, and author profiles for this publication at: <https://www.researchgate.net/publication/263739903>

# Spray Coating of Crack Templates for the Fabrication of Transparent Conductors and Heaters on Flat and Curved Surfaces

ARTICLE in ACS APPLIED MATERIALS & INTERFACES · JULY 2014

Impact Factor: 6.72 · DOI: 10.1021/am503154z · Source: PubMed

---

CITATIONS

5

READS

169

## 6 AUTHORS, INCLUDING:



Ritu Gupta

Indian Institute of Technology Jodhpur

32 PUBLICATIONS 241 CITATIONS

[SEE PROFILE](#)



K.D.M. Rao

Jawaharlal Nehru Centre for Advanced Scien...

13 PUBLICATIONS 71 CITATIONS

[SEE PROFILE](#)



Ankush Kumar

Jawaharlal Nehru Centre for Advanced Scien...

3 PUBLICATIONS 12 CITATIONS

[SEE PROFILE](#)



Giridhar U Kulkarni

Centre for Nano and Soft Matter Sciences

271 PUBLICATIONS 4,439 CITATIONS

[SEE PROFILE](#)

# Spray Coating of Crack Templates for the Fabrication of Transparent Conductors and Heaters on Flat and Curved Surfaces

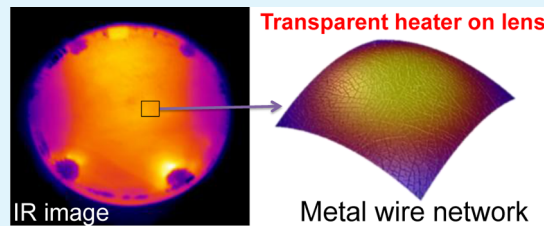
Ritu Gupta,<sup>†</sup> K. D. M. Rao,<sup>†</sup> Kartikeya Srivastava, Ankush Kumar, S. Kiruthika, and Giridhar U. Kulkarni\*

Chemistry & Physics of Materials Unit and Thematic Unit of Excellence in Nanochemistry, Jawaharlal Nehru Centre for Advanced Scientific Research, Jakkur P.O., Bangalore 560 064, India

## Supporting Information

**ABSTRACT:** Transparent conducting electrodes (TCEs) have been made on flat, flexible, and curved surfaces, following a crack template method in which a desired surface was uniformly spray-coated with a crackle precursor (CP) and metal (Ag) was deposited by vacuum evaporation. An acrylic resin (CP1) and a SiO<sub>2</sub> nanoparticle-based dispersion (CP2) derived from commercial products served as CPs to produce U-shaped cracks in highly interconnected networks. The crack width and the density could be controlled by varying the spray conditions, resulting in varying template thicknesses. By depositing Ag in the crack regions of the templates, we have successfully produced Ag wire network TCEs on flat-flexible PET sheets, cylindrical glass tube, flask and lens surface with transmittance up to 86%, sheet resistance below 11 Ω/□ for electrothermal application. When used as a transparent heater by joule heating of the Ag network, AgCP1 and AgCP2 on PET showed high thermal resistance values of 515 and 409 °C cm<sup>2</sup>/W, respectively, with fast response (<20 s), requiring only low voltages (<5 V) to achieve uniform temperatures of ~100 °C across large areas. Similar was the performance of the transparent heater on curved glass surfaces. Spray coating in the context of crack template is a powerful method for producing transparent heaters, which is shown for the first time in this work. AgCP1 with an invisible wire network is suited for use in proximity while AgCP2 wire network is ideal for use in large area displays viewed from a distance. Both exhibited excellent defrosting performance, even at cryogenic temperatures.

**KEYWORDS:** spray coating, crack network, Ag wire, curved electrode, transparent heater, defrosting



## 1. INTRODUCTION

Large-area transparent heaters are of utmost importance in applications such as display panels,<sup>1</sup> touch screens,<sup>2</sup> roof top solar panels,<sup>3</sup> camera lenses, windows, and mirrors that require visual transmittance in cold and moist environmental conditions.<sup>4</sup> Transparent heaters are inevitable where antifogging<sup>5</sup> and deicing<sup>6</sup> is required for the operational stability of the devices. Indium tin oxide (ITO) has long served as an ideal material for transparent heaters, since it has high transmittance (~90%) and low sheet resistance (~10 Ω/□), along with good environmental stability.<sup>7,8</sup> Because of the brittleness associated with ITO, its practical use in flexible devices is challenging.<sup>9</sup> Moreover, its current carrying ability and thermal stability are also limited.<sup>8</sup> With such drawbacks associated with ITO, new materials such as graphene films,<sup>1,10,11</sup> carbon nanotube network films,<sup>12–14</sup> and Ag nanowire networks and grids<sup>15–18</sup> have been developed that can be potential candidates for ITO replacement. Indeed, many ITO-free devices have been reported in recent years, based on the new materials, although mainly in the context of transparent conductors. Only in a few cases, successful fabrication of transparent heaters has been realized.<sup>4,19–23</sup>

Low sheet resistance and high transmittance do not guarantee that a given electrode can be used for transparent heater application. The uniformity of sheet resistance is

essential for homogeneous temperature distribution over large areas.<sup>21</sup> Small surface defects such as pinholes, scratches, and dirt cause nonuniformity of the coating leading to locally high resistance,<sup>24</sup> which can become hotspots and result in failure of the heater. The Ag nanowire networks usually suffer from high resistance at crossbar junctions which, during joule heating, tend to behave as hot spots, leading to local melting.<sup>25</sup> Kim et al. showed that the stability of the Ag nanowire network-based transparent heater can be improved noticeably by avoiding the formation of nanowire aggregates in the network during fabrication.<sup>23</sup> By comparison, transparent graphene conductors seem to do better,<sup>4</sup> although they exhibit relatively high sheet resistance requiring high operating voltages. Thus, low sheet resistance and excellent uniformity over large area are important criteria for a transparent heater. What one desires is a simple and inexpensive method of producing metal wire network-based conductors, uniform over a large area with minimal contact and junction resistances. Here, we make use of the method developed recently by us,<sup>26–29</sup> as well as by Han et al.,<sup>30</sup> in which a dried colloidal layer hosting a spontaneously formed crack network is used as a template for producing a fine

Received: May 21, 2014

Accepted: June 26, 2014

metal wire network, virtually devoid of crossbar wire junctions. In our previous studies,<sup>26–29</sup> we have employed spin coating, drop coating, and rod coating techniques for producing templates. In this study, we have explored the possibility of making a crack template using spray deposition, especially on curved surfaces where common methods such as spin coating may be inconceivable and drop coating may not work well. Spray deposition technique is an attractive tool, because it is one of the most suitable and efficient techniques for low-cost industrial-scale processes.<sup>31</sup> It is already well-established for industrial use and in-line deposition processes. Several TCEs have been fabricated by direct spray coating of Ag nanowires,<sup>32,33</sup> PEDOT:PSS,<sup>34</sup> and graphene oxide dispersion<sup>35</sup> over large areas. Most of these TCEs, however, are limited to flat surfaces.<sup>32–35</sup> The biggest advantage of using spray coating over other techniques is that it ensures uniform coating on complex three-dimensional (3D) curvilinear objects with varying topography.<sup>36</sup> However, there has been little effort in the literature of using spray technique for the fabrication of TCE directly on curved surfaces.<sup>37</sup> Puetz et al. showed the fabrication of transparent oxide electrode by spray coating of antimony-doped tin oxide sol-gel (ATO) on glass tube.<sup>39</sup> In this work, we demonstrate the fabrication of metal-network-based transparent conducting electrodes directly on curved objects by beginning with spray coating of a crackle precursor (CP). Thus, produced transparent heaters are shown to perform as defoggers, even near cryogenic temperatures.

## 2. EXPERIMENTAL SECTION

**Fabrication of Crack Template by Spray Coating.** The crackle precursors (CPs) were chosen such that wide range of crack widths could be obtained. A commercially available crackle nail polish (CP1) consisting of acrylic resin colloidal dispersion (Ming Ni Cosmetics Co., Guangzhou, China) and crackle paint (CP2) consisting of colloidal SiO<sub>2</sub> nanoparticles purchased from Premium Coatings & Chemicals (India) were the two cracking precursors for spray coating. CP1 was diluted to 0.2–0.6 g/mL with the diluter (Ming Ni Cosmetics Co., Guangzhou, China) while CP2 was added with the commercially available diluter and ethyl acetate in 3:1 volume ratio resulting in a concentration of 0.2 g/mL. The dispersions were left overnight in an airtight bottle. The suspended solution were rigorously ultrasonicated for 30 min prior to spray coating. The CPs were spray-deposited using a 135A Airbrush (United Traders, Bangalore) with a 0.2 mm nozzle held at a fixed distance of ~3 cm above the surface at a nitrogen pressure of ~10 psi. The spray coating was done under constant ambient conditions (25 °C and RH of 45%). Ag metal deposition was carried out on curved objects uniformly inside a physical vapor deposition system (Hindvac, India). A 55 V AC bias was applied to a tungsten basket containing ~150 mg of Ag ingot at a base pressure of 10<sup>-6</sup> Torr to vacuum evaporate Ag metal. The substrates were held at a distance using a custom designed automated rotating holder (2 rotations per second). The deposition is done for 10 min to result in film thickness of ~80 nm.

**Characterization.** A Wyko NT9100 Optical Profiling System (Bruker, USA) was used for height and depth measurements of the coatings. Energy-dispersive spectroscopy (EDS) analysis was performed with an EDAX Genesis instrument (Mahwah, NJ) attached to the scanning electron microscopy (SEM) column. Transmittance spectra were taken using a Perkin–Elmer Model Lambda 900 UV/visible/near-IR spectrophotometer with a white light source coupled with a monochromator and detected using integrating sphere and a Si photodiode. Sheet resistance was measured using a 4-point probe station (Techno Science Instruments, India). Image-J software was used to perform analysis of the crack patterns.

In situ thermal images of the Ag patterned electrodes while applying voltage was captured using a thermal imager (Testo 885-2, USA) with

640 × 480 pixels, a thermal sensitivity of 0.03 °C, a 30° field of view covering the long wavelength infrared spectral range of 8–14 μm. The imager also provides relative surface humidity maps based on the ambient temperature, humidity and surface temperature values. The thermal images were acquired from the back side of the electrodes. The data points for temperature profile was obtained from the clip recorded during the measurement. A digital multimeter with DMM Viewer was used for recording the resistance changes with time.

## 3. RESULTS AND DISCUSSION

In the spray deposition process, there are many controllable variables such as solvent, solution viscosity, spray pressure, spray distance from sample, spray time, and number of spray coats, and all can influence the coating.<sup>38</sup> The ink formulation and the solvent properties such as vapor pressure, nozzle flow rate, viscosity, and surface tension, also play an important role in deciding the overall quality of coating.<sup>39</sup> The crackle precursors (CPs) were diluted suitably (see the Experimental Section) such that clogging of the airbrush is avoided. The fabrication of the crack template on a curved surface is schematically shown in Figure 1a. The curved objects were coated with crackle precursor CP1, using a custom-designed spray-coating setup mounted on a holder, as shown in Figure 1b. The tube is uniformly coated with cracks all around its diameter. Similarly, a curved convex lens coated with CP1 at a single spray pass and air pressure of 10 psi is shown in Figure

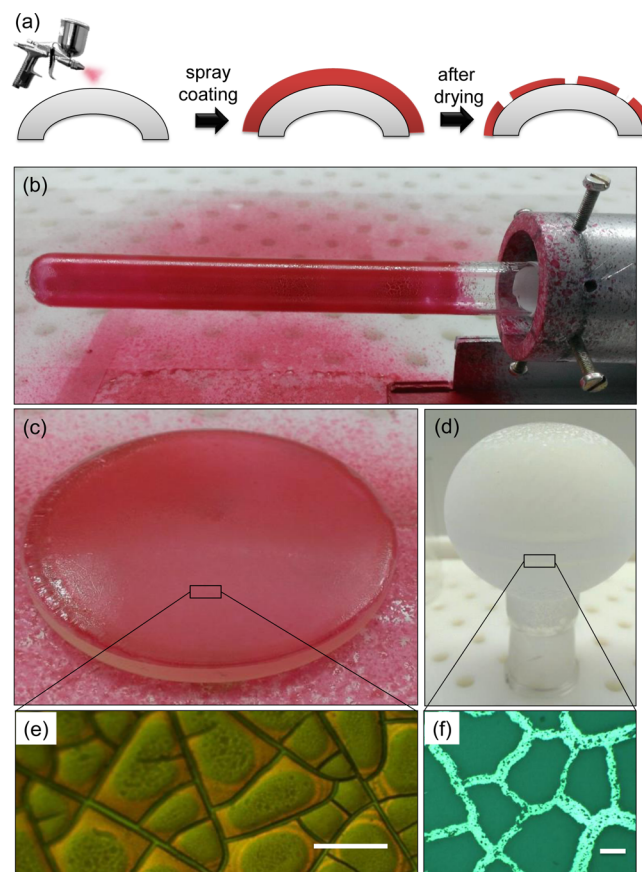


**Figure 1.** (a) Schematic illustration of the fabrication of crack template on curved surface by spray coating. Photograph demonstrating spray coating of crackle precursor CP1 on (b) glass tube and (c) convex lens, while (d) CP2 on a round-bottom flask is shown. Optical microscope images of crack template formed on (e) lens surface (scale bar = 50 μm) and (f) flask surface (scale bar = 100 μm).

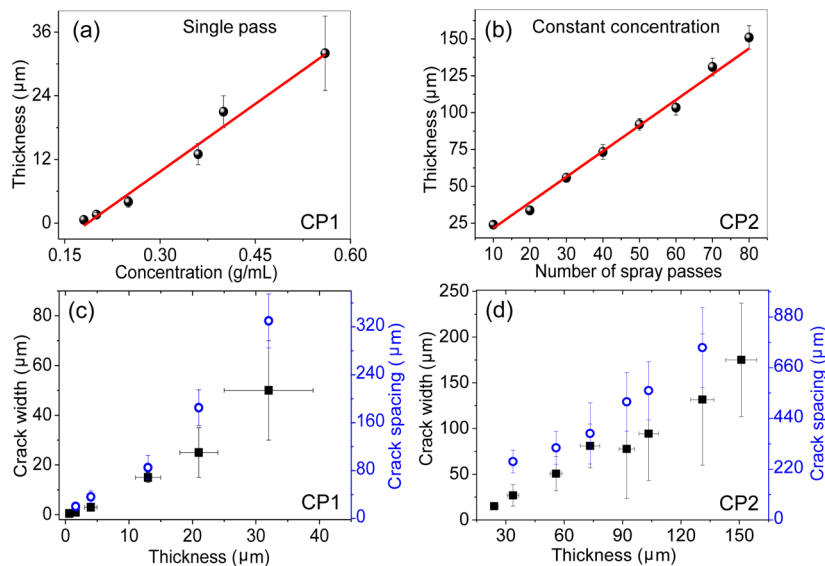


**Figure 2.** Thickness variation in dried crack layer obtained by spray coating for (a) different concentrations of CP1 in a single spray pass and (b) various numbers of spray passes for a fixed concentration (0.2 g/mL) in case of CP2. Variations in crackle features with respect to crack thickness for (c) CP1 and (d) CP2.

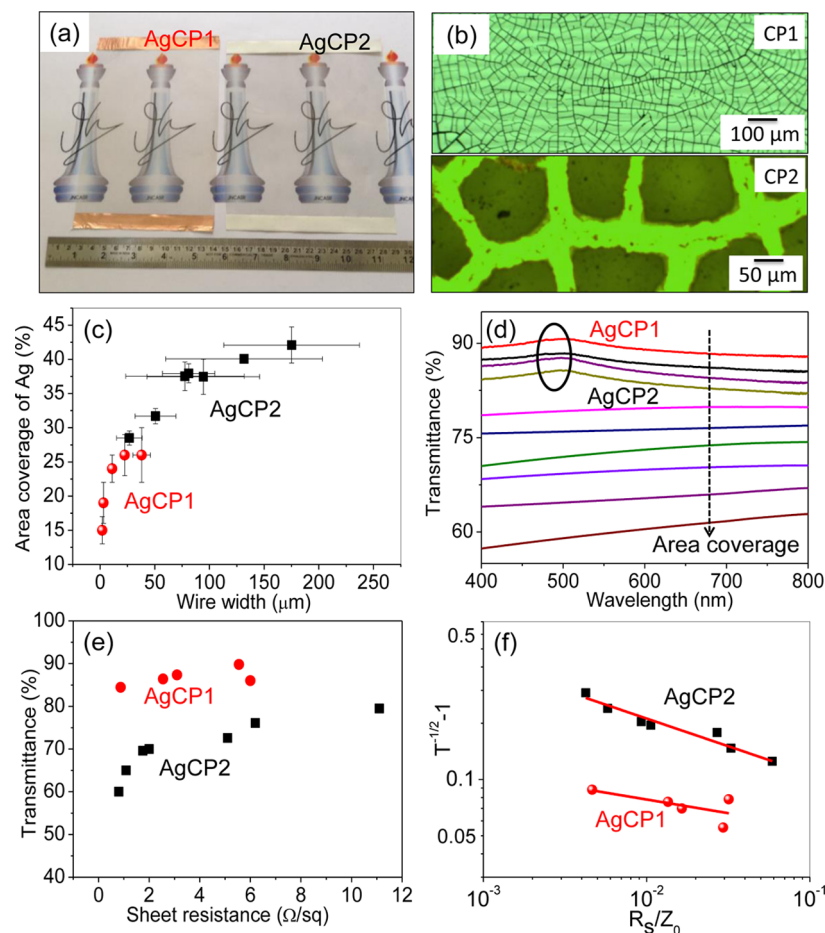


**Figure 3.** (a) Photograph and (b) optical micrographs of the Ag wire networks (AgCP1 and AgCP2). (c) Area coverage of Ag wire networks for various wire widths obtained in AgCP1 and AgCP2. (d) Transmittance spectra for AgCP1 (encircled) and AgCP2. (e) Transmittance versus sheet resistance for AgCP1 and AgCP2. (f)  $T^{-1/2} - 1$  vs  $R_s/Z_0$  plot for the data given in panel e. (Here, the red circles represent AgCP1 and the black squares represent AgCP2.)

1c. The self-drying of the spray-coated film in ambient condition resulted in a crack network, as shown in Figure 1d.

Similarly, CP2 was also coated on curved objects such as a round-bottom flask (Figure 1d) where an interconnected crack

network formed upon slow drying, as shown in Figure 1e. It may be noted that crackle precursor CP2 took a longer time ( $\sim 90$  min) for complete drying, compared to CP1, which dried off quickly within  $\sim 5$  min, and that the cracks in CP1 are much finer in contrast to those from CP2 (see Figure S1 in the Supporting Information for more details). Importantly, we are able to achieve cracks down to the substrate (to distinguish from incomplete cracks,<sup>40</sup> we term these as crackles), which is important for use as a template (see 3D profilometry image in Figure S2 in the Supporting Information).

After having realized the possibility of obtaining crack networks on curved objects by spray coating, we optimized the crack template formation on flat PET substrate, by tuning the solution concentration and number of spray passes for CP1 and CP2 crackle precursors, respectively. Since CP1 is fast evaporating, we chose to spray coat in a single pass and achieve the desired thickness by varying its concentration (0.2–0.6 g/mL), however, without causing any clogging of the airbrush. The thickness of the dried film varied linearly between 0.5–30  $\mu\text{m}$  for the range of dilution employed (see Figure 2a). The CP2 crackle precursor is relatively viscous even at low concentrations and thus required several spray passes for building up the layer thickness. Nearly 10 passes of spray over the same region resulted in a thickness of  $\sim 24 \pm 2 \mu\text{m}$  but it did not crack properly. The number of spray passes was increased gradually to 80 resulting in a dried crack template thickness of  $150 \pm 5 \mu\text{m}$  (Figure 2b). From Figures 2a and 2b, it is clear that spray coating method of forming the crack template provides a good control over the layer thickness, similar to rod coating.<sup>26</sup> However, the latter is not easily applicable to curved surfaces. The drop coating technique could be adapted to curved surfaces, but uniformity in coating over large area can not be assured.<sup>29</sup>

For both crackle precursors, there is a critical thickness below which cracking does not occur. The threshold thickness of CP1 was found to be  $\sim 800$  nm while for CP2, this threshold thickness is  $\sim 30 \mu\text{m}$ . The difference in the critical thickness for cracking depends on the nature of crackle dispersion, particle type, size, solvent, etc.<sup>41</sup> Since the nature of cracking is different for the two precursors, we are provided with a wider range of crack patterns, which is advantageous in different contexts (vide infra). The SEM characterization of particle size and morphology can be seen in Figure S3 in the Supporting Information. The CP1 precursor contains soft acrylic particles ( $\sim 50$  nm) that may partially release the stress developed during drying by deforming, while the remaining stress is being released via crack formation.<sup>41</sup> Thus, CP1 results in the formation of much finer cracks, ranging between 2  $\mu\text{m}$  and 40  $\mu\text{m}$  (see Figure 2c and Figure S4 in the Supporting Information) with low layer thicknesses. Since the CP2 precursor consists of hard silica particles ( $<20$  nm), particle deformation in this case may be negligible and, therefore, all the stress developed in the layer during drying is released only via crack formation. Thus, much wider cracks (30–250  $\mu\text{m}$ ) get formed at higher film thicknesses, as seen in Figure 2d and Figure S4 in the Supporting Information. For both precursors CP1 and CP2, the crack width and spacing bear a direct relation with the thickness of the crack template, which is well-known in crack physics.<sup>42</sup>

The crack templates were deposited with Ag metal  $\sim 80$  nm thick, and the templates were then removed by lift-off (see schematic in Figure S5 in the Supporting Information). The Ag wire networks formed using CP1 and CP2 templates are

termed as AgCP1 and AgCP2, respectively. The photographs of AgCP1 (12 cm  $\times$  18 cm) and AgCP2 (14 cm  $\times$  18 cm) patterned PET are shown in Figure 3a. The optical micrographs reveal the connectivity of Ag wire network for AgCP1 and AgCP2 (see Figure 3b). The metal fill factors (percentage metal area coverage) in Figure 3b are 24% and 42%, respectively, for AgCP1 and AgCP2, which varied with respect to the wire width. As seen in Figure 3c, the fill factor of AgCP1 is less (15%–25%), compared to that of AgCP2 (28%–42%), as wires are narrower in the former case. A low metal coverage is important in electrodes requiring high transmittance while high metal coverage ensures good conductivity across the electrode. Thus, the spray coated templates developed in this study not only provide a choice of wire widths in a broad range (2–250  $\mu\text{m}$ ), but also enable TCE fabrication over large areas. The transmittance spectra have been measured in specular mode for both types of Ag electrodes (Figure 3d). The AgCP1 electrodes exhibit high transmittance (up to 88%). The diffuse transmittance including the contribution of scattered light was found to be more than the specular transmittance resulting in haze of  $\sim 5\%$  (see Figure S6 in the Supporting Information). The transmission at 550 nm for Ag electrodes with different area coverages is plotted as a function of sheet resistance in Figure 3e. The sheet resistance values are quite low ( $<11 \Omega/\square$ ) for all the electrodes, while the transmittance was above 80% for AgCP1 and  $\sim 60\%-78\%$  for AgCP2 electrodes. The low sheet resistance is a result of seamless wire junctions, which we have discussed in detail in our early work.<sup>29</sup> A TCE is quantitatively accessed usually by the figure of merit (FoM). There are several ways of defining FoM,<sup>24</sup> the most popular one is  $\sigma_{\text{OP}}/\sigma_{\text{DC}}$  (ratio of DC and optical conductivities), which relate  $T$  with  $R_s$  for conducting thin films using eq 1:

$$T = \left[ 1 + \left( \frac{z_0 \sigma_{\text{OP}}}{2R_s \sigma_{\text{DC}}} \right) \right]^{-2} \quad (1)$$

The  $\sigma_{\text{OP}}/\sigma_{\text{DC}}$  values fall in the range of 400 to 2445 for AgCP1 and 482 to 809 in the case of AgCP2. The values obtained here are commendable and, to our knowledge, probably the highest reported in the literature (see Table S1 in the Supporting Information). Recently, Han et al. claimed high values of  $\sigma_{\text{OP}}/\sigma_{\text{DC}}$  in the range of 300–700 for Ag wire networks.<sup>30</sup> With our networks, we could achieve much higher values probably due to lower metal fill factor and lesser haze ( $\sim 5\%$ ). In order to understand the conduction behavior of these networks, the following equation (eq 2), given by Sorel et al.,<sup>43</sup> was used to fit the data in Figure 3e.

$$T = \left[ 1 + \frac{1}{\Pi} \left( \frac{z_0}{R_s} \right)^{1/(n+1)} \right]^{-2} \quad (2)$$

where  $\Pi$  is the percolative figure of merit and  $n$  is the percolative exponent. From the fits in Figure 3f, the fitting parameters for AgCP1 are  $\Pi = 25.6$  and  $n = 5.8$ , and for AgCP2, the values are  $\Pi = 18.4$  and  $n = 2.3$ . These values stand above the threshold requirement of industry standards<sup>44</sup> (see Figure 5 of ref 39).

The exceptional optoelectronic properties of the spray-produced electrodes have been further explored by fabricating transparent heaters, initially on PET before embarking on rigid curved surfaces. The electrodes were initially examined for stability against atmospheric oxidation by externally heating at

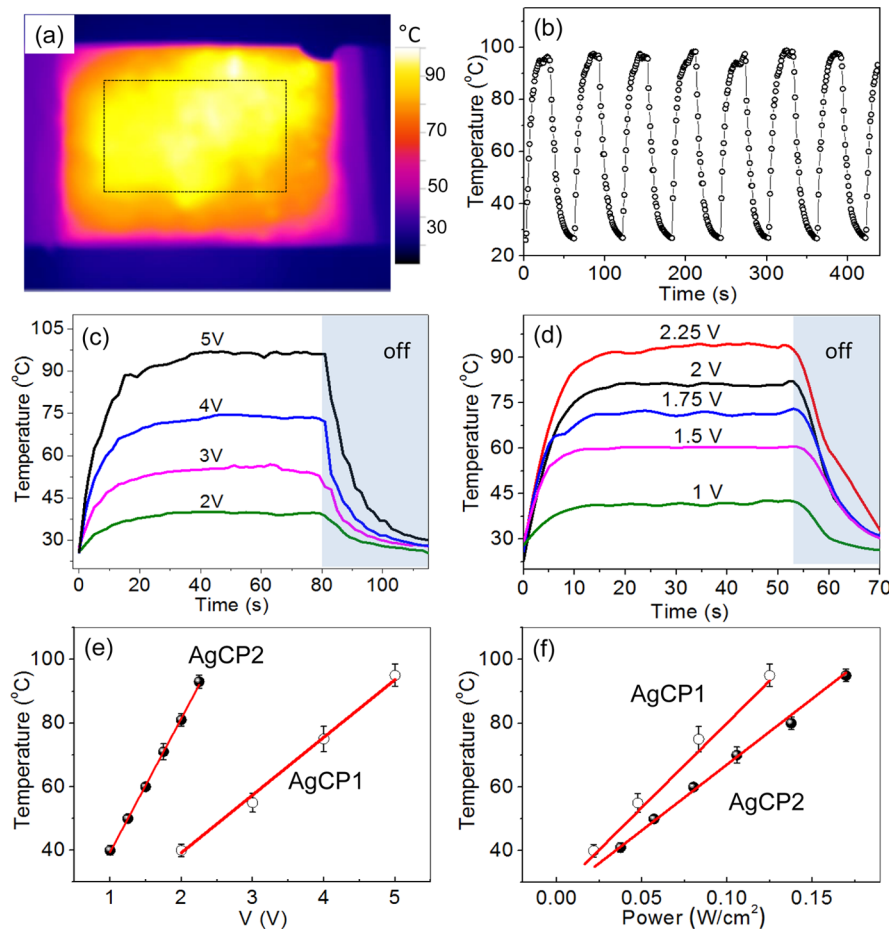


**Figure 4.** (a) Thermal image of an AgCP2-based heater. The temperature distribution in the marked region is shown in Figure S8 in the Supporting Information. (b) Heating cycles at an operating voltage of 2.25 V. Temperature rise curves at different applied voltages, as a function of time for (c) AgCP1 and (d) AgCP2. Maximum temperature attained as a function of (e) applied voltage and (f) input power for both types of electrodes.

**Table 1. Optoelectronic and Thermal Properties of TCEs Derived from Crackle Precursors CP1 and CP2**

pattern type	width ( $\mu\text{m}$ )	cell size ( $\mu\text{m}$ )	T (%)	$R_s$ ( $\Omega/\square$ )	area ( $\text{cm}^2$ )	thermal resistance ( $^\circ\text{C cm}^2/\text{W}$ )	response time (s)	$\Delta T/\Delta V$ ( $^\circ\text{C/V}$ )
AgCP1	2–5	~50	86	6	4 $\times$ 3	515	20	18
AgCP2	100–150	~500	70	2	4 $\times$ 2	409	14	42

different temperatures as well as by monitoring the change in resistance at a given temperature (see Figure S7 in the Supporting Information). The electrodes were then joule-heated by applying a DC bias. A typical thermal image obtained for the AgCP2 network over a  $4\text{ cm} \times 2\text{ cm}$  area is shown in Figure 4a. The area marked in the photograph has a mean temperature of  $93.4 \pm 3.2$  °C. The uniform temperature distribution clearly indicates the high quality of these electrodes (see histogram distribution in Figure S8 in the Supporting Information). The thermal distribution is unaffected, even upon bending, which is only observed for high-performance electrodes (see Figure S9 in the Supporting Information). A voltage of 2.25 V was applied to raise the temperature to 95 °C and after 30 s, it was reduced to zero; this was repeated for several cycles. Accordingly, the temperature switched between ambient (27 °C) and 95 °C, as shown in Figure 4b. Curves showing the rise and fall of the temperature were obtained at different voltages for AgCP1 and AgCP2 (see Figures 4c and 4d). Since the resistance of AgCP2 is lesser because of the higher metal area coverage, temperatures up to 100 °C could be attained at much lower voltages (below 3 V), compared to AgCP1. The

temperature is found to be quite stable under an applied voltage and decreases immediately as soon as the voltage is reduced to zero. The response time is very low (20 and 15 s, respectively, for AgCP1 and AgCP2), compared to the literature results (see Table S2 in the Supporting Information), which may be attributed to less scattering, since the wire junctions are seamless. The power dissipated in the network, given by  $V^2/R$ , indicates that, at a constant voltage, the power is inversely related to resistance. Since the resistance of AgCP2 is lower than AgCP1, higher temperatures are attained at a much lower voltage, as seen from Figure 4e. For large-area heating applications, AgCP2 is preferred since the network parameters—wire width and cell size—are much larger than those in the AgCP1 electrode. This, in turn, is reflected in the low input voltage ( $\Delta T/\Delta V$ ) requirement. The response is also slightly better in the former (see Table 1). For smaller areas that require complete visible transparency, AgCP1 is better, even though it requires a somewhat higher response time and voltage input; it may be noted that these values are however much smaller than those reported in the literature (see Table S2 in the Supporting Information). The choice of CP1 or CP2 for

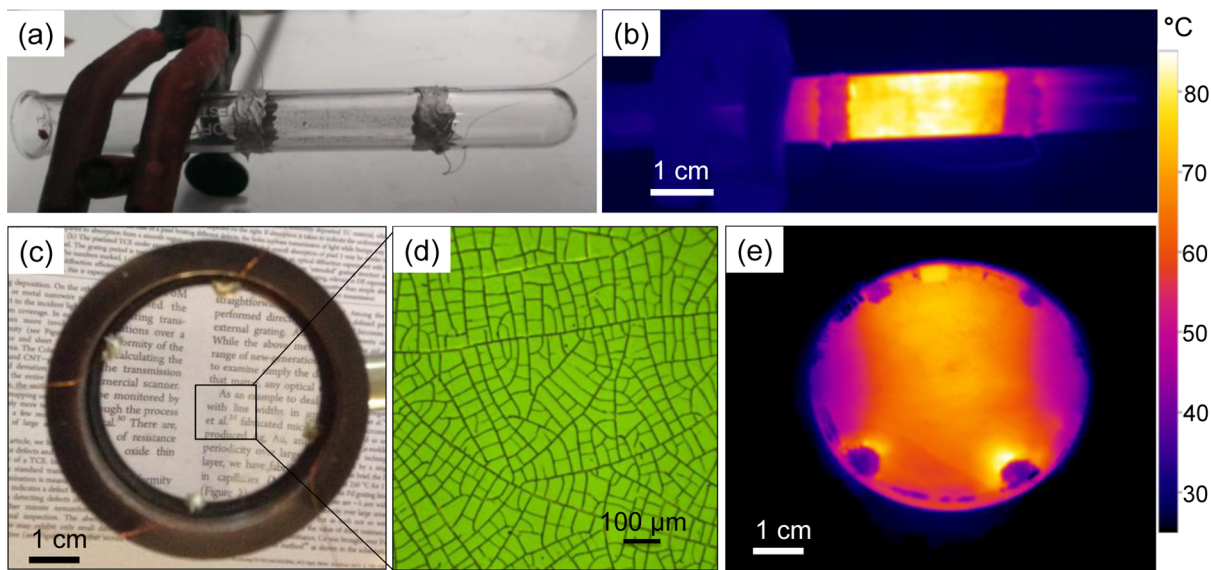


**Figure 5.** (a) Photograph and (b) thermal image of a glass tube covered with AgCP1 at 8 V. (c) A photograph showing the zoom-in text seen clearly through a AgCP1-derived TCE on a convex lens, along with (d) its optical micrograph and (e) its thermal image taken at 9 V.

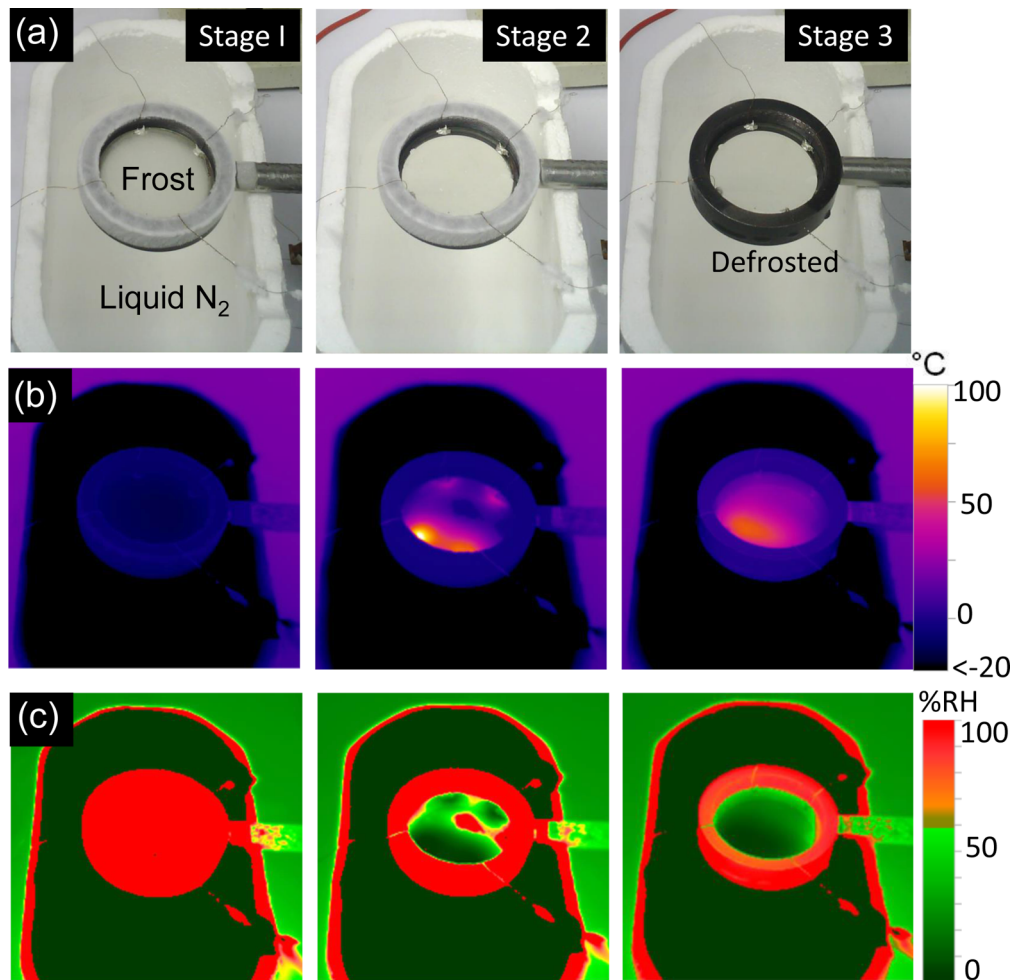


**Figure 6.** (a) Photographs, (b) thermal images, and (c) humidity images of the AgCP1-coated lens, showing the sequential defrosting stages. Initially, in stage 1, frost formed by exposing the TCE (lens) to liquid nitrogen vapor, which, upon applying a voltage of 6 V, was partially removed within few seconds (stage 2), and after 2 min (stage 3), complete removal of the frost occurred.

patterning is dependent on the specific application under consideration. The thermal resistance calculated from the

slopes of temperature-versus-power plots<sup>45</sup> (Figure 4f) is determined to be 515 °C cm<sup>2</sup>/W and 409 °C cm<sup>2</sup>/W for

AgCP1 and AgCP2, respectively. These values are much higher, compared to literature results on Ag nanowire and CNT-based TCEs, which is understandable, since the present TCEs do not suffer from a loss at the junctions. Indeed, the values are comparable to that obtained with graphene-based transparent heaters (see Table S2 in the Supporting Information).

The transparent heaters find high practical utility when fabricated on substrates of any curvature. Although ITO coating on curved surfaces is well-known,<sup>46</sup> this issue is not well-addressed in the literature, particularly in the context of new-generation TCEs. The CP spray-coated directly on curved objects was developed after depositing metal (thickness of ~80 nm) with the help of a custom-designed setup for rotating the object inside the chamber during deposition (see Figure 1b). Figures 5a and 5c show the AgCP1 metal networks fabricated on a glass tube and a convex lens, respectively. By applying 8 V to ring electrodes, the tube could be made to attain a temperature of ~85 °C uniformly all around its curvature (see Figure 5b). Such transparent heaters may find applications in culturing of cells, biomonitoring and chemical reactions, where uniform heating is required at a constant temperature. The AgCP1 coated on a convex lens presents another example, where these patterns are invisible to the naked eye. The text letters below the lens are clearly seen magnified through the lens (Figure 5c), despite the surface being patterned with wire network, as seen in the optical microscope image in Figure 5d. The lens was joule-heated by taking contacts from the four corners such that the uniform temperature distribution is achieved (see Figure 5e). Thus, this spray-coating technique is able to produce uniform wire networks on curved objects as well.

The heating performance of the AgCP1-coated lens was utilized for defrosting, as shown in Figure 6a. The frost formed by freezing over liquid nitrogen disappeared quickly upon applying a voltage (6 V) *in situ* for 2 min, as indicated by stages 1, 2, and 3. The thermal images in Figure 6b show the corresponding temperature changes on the defrosted lens surface. The temperature above the liquid nitrogen bath was less than -20 °C while the lens surface showed a temperature of 0 °C (stage 1). As the voltage was turned on in stage 2, the temperature started to rise, as seen more clearly at the contacts. After complete defrosting (stage 3), the temperature reached a value higher than the surroundings, as clearly seen in the defrosted image. To examine further, relative surface humidity maps were obtained from the thermal imager, as shown in Figure 6c. The ambient humidity was ~48%, while above liquid nitrogen bath, it was nearly 0%, as nitrogen filled the local atmosphere. The frosted lens surface appears red with 100% RH (left) due to frost formation, which, upon heating, changed to the ambient RH, because of defrosting (see middle and right images). This shows the capability of a transparent heater to work, even at subzero operating temperatures.

Thus, spray coating of crack template is a viable and efficient route to TCE fabrication, particularly on curved surfaces. Using the spray coating method, the desired template thickness can be easily achieved, even on highly curved surfaces, and it is the thickness alone that ultimately decides the nature of the crack network and, in turn, the nature of the wire network on the curved TCE. This clearly is the merit of the present method. On the other hand, spray coating of nanowire dispersions to produce TCEs is indeed possible but is limited to flat substrates.<sup>32,33</sup> Otherwise, it is shown that a prefabricated TCE on a flat substrate can be transferred onto a curved object

using a polymer support.<sup>47,48</sup> However, transferability over large area involving complex surfaces can prove difficult. A flexible sheet cannot be laminated perfectly on a curved surface without cuts and folds. Furthermore, lamination on curved objects will not produce a continuous network but rather artificially connected TCE fragments. This may also introduce extra electrical junctions and relatively less-transparent regions between the TCE fragments. The transfer substrate (a polymer usually) adds additional thermal mass with poor thermal conductivity. Thus, the power required to heat up the curved surface will be much greater, because of an additional heat sink. The lamination may require adhesive between components whose optical and thermal properties may interfere with the defrosting action and degrade the performance. Such shortcoming are completely avoided in the present method. Where the TCE is directly fabricated on the curved tube surface, for example, by ATO coating, the sheet resistance is comparatively higher ( $R_s = 3\text{--}5 \text{ k}\Omega/\square$ ) which may not result in an ideal heater.<sup>37</sup> In our method, the metal wire network is produced directly on the curved surface and is seamless with low sheet resistance. The fabricated transparent heater exhibited high performance, in terms of uniformity of heating, operating voltages, and stability. The temperature rise and fall typically occurs within less than a minute during heating and cooling, which is an important characteristic for a heater. These features of a transparent heater may not be easily achievable using other materials and methods (see Table S2 in the Supporting Information).

## CONCLUSIONS

In conclusion, we have developed a method of spray coating of crackle precursor for fabricating a crack template on flat and curved surfaces to obtain crack networks, which serve as sacrificial templates for depositing metal wire networks. In essence, we have extended a well-established method in our laboratory,<sup>26</sup> to curved surfaces involving spray coating. The process is highly scalable. Compared to other deposition methods,<sup>26</sup> physical metal deposition is neat and well-controlled. Two types of crackle precursors—one based on acrylic resin (CP1) and another based on SiO<sub>2</sub> particles (CP2)—were chosen such that the crack widths spanning from 2 to 250 μm were made with fill factors in the range of 15%–42%, the lower values pertaining to AgCP1 and the higher values pertaining to AgCP2. The crack template was obtained on curved objects such as tubes, lenses, and flasks, as well as on flat and flexible substrates. The obtained metal wire networks simply mimic the crack networks: those resulting from AgCP1 were invisible, even from small viewing distances, while those from AgCP2 were unnoticeable from a distance. Importantly, both showed excellent optoelectronic properties, such as low sheet resistance and high transmittance (6 Ω/□ at 86% for AgCP1; 2 Ω/□ at 70% for AgCP2). Using AgCP1 and AgCP2, transparent heaters have been fabricated on flat-flexible PET as well as on curved glass objects, resulting in uniform heating all across, irrespective of the substrate type and its curvature. Thus, made transparent heaters were high performing exhibiting low response times (<20 s), low input voltages (<5 V), and thermal resistances as high as 515 °C cm<sup>2</sup>/W. Upon application of a nominal voltage of 6 V, a temperature of 60 °C was achieved on the lens held under subzero Celsius conditions. This is clearly an exceptional performance, with regard to defrosting at cryogenic temperatures.

## ASSOCIATED CONTENT

### Supporting Information

Change in the volume of the crackle precursor during drying, SEM images of dried colloidal dispersions, optical micrographs and optical profiler images of crack templates, schematic illustration of metal wire network fabrication, specular and diffusive transmission from AgCP1, the resistance variation upon external heating, histogram showing temperature distribution of AgCP1, thermal images of AgCP2 at bent position and literature comparison of transparent conducting electrode and transparent heaters. This material is available free of charge via the Internet at <http://pubs.acs.org>.

## AUTHOR INFORMATION

### Corresponding Author

\*E-mail: kulkarni@jncasr.ac.in.

### Author Contributions

<sup>†</sup>Both authors contributed equally to this work.

### Notes

The authors declare no competing financial interest.

## ACKNOWLEDGMENTS

The financial support from DST, India is gratefully acknowledged. The authors thank Prof. C. N. R. Rao for his encouragement. K.D.M.R. acknowledges UGC for fellowship, and S.K. acknowledges Inspire for their fellowship. R.G. thanks Sunil Walia for assistance.

## REFERENCES

- (1) Bae, S.; Kim, H.; Lee, Y.; Xu, X.; Park, J. S.; Zheng, Y.; Balakrishnan, J.; Lei, T.; Ri Kim, H.; Song, Y. I.; Kim, Y. J.; Kim, K. S.; Ozylmaz, B.; Ahn, J. H.; Hong, B. H.; Iijima, S. Roll-to-Roll Production of 30-in. Graphene Films for Transparent Electrodes. *Nat. Nanotechnol.* **2010**, *5*, 574–578.
- (2) Pang, S.; Hernandez, Y.; Feng, X.; Müllen, K. Graphene as Transparent Electrode Material for Organic Electronics. *Adv. Mater.* **2011**, *23*, 2779–2795.
- (3) Shah, A. V.; Sculati-Meillaud, F.; Berenyi, Z. J.; Ghahfarokhi, O. M.; Kumar, R. Diagnostics of Thin-Film Silicon Solar Cells and Solar Panels/Modules with Variable Intensity Measurements (VIM). *Sol. Energy Mater. Sol. Cells* **2011**, *95*, 398–403.
- (4) Bae, J. J.; Lim, S. C.; Han, G. H.; Jo, Y. W.; Doung, D. L.; Kim, E. S.; Chae, S. J.; Huy, T. Q.; Van Luan, N.; Lee, Y. H. Heat Dissipation of Transparent Graphene Defoggers. *Adv. Funct. Mater.* **2012**, *22*, 4819–4826.
- (5) Chen, Y.; Zhang, Y.; Shi, L.; Li, J.; Xin, Y.; Yang, T.; Guo, Z. Transparent Superhydrophobic/Superhydrophilic Coatings for Self-Cleaning and Anti-Fogging. *Appl. Phys. Lett.* **2012**, *101*, 033701.
- (6) Kang, J.; Kim, H.; Kim, K. S.; Lee, S. K.; Bae, S.; Ahn, J. H.; Kim, Y. J.; Choi, J. B.; Hong, B. H. High-Performance Graphene-Based Transparent Flexible Heaters. *Nano Lett.* **2011**, *11*, 5154–5158.
- (7) Kim, H.; Gilmore, C. M.; Pique, A.; Horwitz, J. S.; Mattoussi, H.; Murata, H.; Kafafi, Z. H.; Chrisey, D. B. Electrical, Optical, and Structural Properties of Indium-Tin-Oxide Thin Films for Organic Light-Emitting Devices. *J. Appl. Phys.* **1999**, *86*, 6451–6461.
- (8) Noh, J. H.; Lee, S.; Kim, J. Y.; Lee, J. K.; Han, H. S.; Cho, C. M.; Cho, I. S.; Jung, H. S.; Hong, K. S. Functional Multilayered Transparent Conducting Oxide Thin Films for Photovoltaic Devices. *J. Phys. Chem. C* **2008**, *113*, 1083–1087.
- (9) Zhou, Y.; Cheun, H.; Choi, S.; Potscavage, W. J.; Fuentes-Hernandez, C.; Kippelen, B. Indium Tin Oxide-Free and Metal-Free Semitransparent Organic Solar Cells. *Appl. Phys. Lett.* **2010**, *97*, 153304.
- (10) Geim, A. K.; Novoselov, K. S. The Rise of Graphene. *Nat. Mater.* **2007**, *6*, 183–191.
- (11) Becerril, H. C. A.; Mao, J.; Liu, Z.; Stoltzenberg, R. M.; Bao, Z.; Chen, Y. Evaluation of Solution-Processed Reduced Graphene Oxide Films as Transparent Conductors. *ACS Nano* **2008**, *2*, 463–470.
- (12) Kim, Y. H.; Muller-Meskamp, L.; Zakhidov, A. A.; Sachse, C.; Meiss, J.; Bikova, J.; Cook, A.; Zakhidov, A. A.; Leo, K. Semi-Transparent Small Molecule Organic Solar Cells with Laminated Free-Standing Carbon Nanotube Top Electrodes. *Sol. Energy Mater. Sol. Cells* **2012**, *96*, 244–250.
- (13) Zhang, D.; Ryu, K.; Liu, X.; Polikarpov, E.; Ly, J.; Tompson, M. E.; Zhou, C. Transparent, Conductive, and Flexible Carbon Nanotube Films and their Application in Organic Light-Emitting Diodes. *Nano Lett.* **2006**, *6*, 1880–1886.
- (14) King, P. J.; Higgins, T. M.; De, S.; Nicoloso, N.; Coleman, J. N. Percolation Effects in Supercapacitors with Thin, Transparent Carbon Nanotube Electrodes. *ACS Nano* **2012**, *6*, 1732–1741.
- (15) De, S.; Higgins, T. M.; Lyons, P. E.; Doherty, E. M.; Nirmalraj, P. N.; Blau, W. J.; Boland, J. J.; Coleman, J. N. Silver Nanowire Networks as Flexible, Transparent, Conducting Films: Extremely High DC to Optical Conductivity Ratios. *ACS Nano* **2009**, *3*, 1767–1774.
- (16) Hu, L.; Kim, H. S.; Lee, J. Y.; Peumans, P.; Cui, Y. Scalable Coating and Properties of Transparent, Flexible, Silver Nanowire Electrodes. *ACS Nano* **2010**, *4*, 2955–2963.
- (17) Gaynor, W.; Burkhard, G. F.; McGehee, M. D.; Peumans, P. Smooth Nanowire/Polymer Composite Transparent Electrodes. *Adv. Mater.* **2011**, *23*, 2905–2910.
- (18) Gupta, R.; Hösel, M.; Jensen, J.; Krebs, F. C.; Kulkarni, G. U. Digital Grayscale Printing for Patterned Transparent Conducting Ag Electrodes and their Applications in Flexible Electronics. *J. Mater. Chem. C* **2014**, *2*, 2112–2117.
- (19) Celle, C.; Mayousse, C. I.; Moreau, E. O.; Basti, H.; Carella, A.; Simonato, J. P. Highly Flexible Transparent Film Heaters Based on Random Networks of Silver Nanowires. *Nano Res.* **2012**, *5*, 427–433.
- (20) Janas, D.; Koziol, K. A Review of Production Methods of Carbon Nanotube and Graphene Thin Films for Electrothermal Applications. *Nanoscale* **2014**, *6*, 3037–3045.
- (21) Kang, J.; Kim, H.; Kim, K. S.; Lee, S. K.; Bae, S.; Ahn, J. H.; Kim, Y. J.; Choi, J. B.; Hong, B. H. High-Performance Graphene-Based Transparent Flexible Heaters. *Nano Lett.* **2011**, *11*, 5154–5158.
- (22) Gupta, R.; Walia, S.; Hosel, M.; Jensen, J.; Angmo, D.; Krebs, F. C.; Kulkarni, G. U. Solution Processed Large Area Fabrication of Ag Patterns as Electrodes for Flexible Heaters, Electrochromics and Organic Solar Cells. *J. Mater. Chem. A* **2014**, *2*, 10930–10937.
- (23) Kim, T.; Kim, Y. W.; Lee, H. S.; Kim, H.; Yang, W. S.; Suh, K. S. Uniformly Interconnected Silver-Nanowire Networks for Transparent Film Heaters. *Adv. Funct. Mater.* **2013**, *23*, 1250–1255.
- (24) Gupta, R.; Kulkarni, G. U. Holistic Method for Evaluating Large Area Transparent Conducting Electrodes. *ACS Appl. Mater. Interfaces* **2013**, *5*, 730–736.
- (25) Khaligh, H. H.; Goldthorpe, I. A. Failure of Silver Nanowire Transparent Electrodes under Current Flow. *Nanoscale Res. Lett.* **2013**, *8*, 235.
- (26) Kiruthika, S.; Gupta, R.; Rao, K. D. M.; Chakraborty, S.; Padmavathy, N.; Kulkarni, G. U. Large Area Solution Processed Transparent Conducting Electrode Based on Highly Interconnected Cu Wire Network. *J. Mater. Chem. C* **2014**, *2*, 2089–2094.
- (27) Rao, K. D. M.; Kulkarni, G. U. Highly Crystalline Single Au Wire Network as High Temperature Transparent Heater. *Nanoscale* **2014**, *6*, 5645–5651.
- (28) Kiruthika, S.; Rao, K. D. M.; Kumar, A.; Gupta, R.; Kulkarni, G. U. Metal Wire Network based Transparent Conducting Electrodes Fabricated Using Interconnected Crackled Layer as Template. *Mater. Res. Express* **2014**, *1*, 026301.
- (29) Rao, K. D. M.; Gupta, R.; Kulkarni, G. U. Fabrication of Large Area, High-Performance, Transparent Conducting Electrodes using a Spontaneously Formed Crackle Network as Template. *Adv. Mater. Interfaces* **2014**, DOI: 10.1002/admi.201400090 (accessed June 18, 2014).
- (30) Han, B.; Pei, K.; Huang, Y.; Zhang, X.; Rong, Q.; Lin, Q.; Guo, Y.; Sun, T.; Guo, C.; Carnahan, D.; Giersig, M.; Wang, Y.; Gao, J.;

Ren, Z.; Kempa, K. Uniform Self-Forming Metallic Network as a High-Performance Transparent Conductive Electrode. *Adv. Mater.* **2014**, *26*, 873–877.

(31) Assad, O.; Leshansky, A. M.; Wang, B.; Stelzner, T.; Christiansen, S.; Haick, H. Spray-Coating Route for Highly Aligned and Large-Scale Arrays of Nanowires. *ACS Nano* **2012**, *6*, 4702–4712.

(32) Kim, T.; Canlier, A.; Kim, G. H.; Choi, J.; Park, M.; Han, S. M. Electrostatic Spray Deposition of Highly Transparent Silver Nanowire Electrode on Flexible Substrate. *ACS Appl. Mater. Interfaces* **2012**, *5*, 788–794.

(33) Hauger, T. C.; Al-Rafia, S. M. I.; Buriak, J. M. Rolling Silver Nanowire Electrodes: Simultaneously Addressing Adhesion, Roughness, and Conductivity. *ACS Appl. Mater. Interfaces* **2013**, *5*, 12663–12671.

(34) Tait, J. G.; Worfolk, B. J.; Maloney, S. A.; Hauger, T. C.; Elias, A. L.; Buriak, J. M.; Harris, K. D. Spray Coated High-Conductivity PEDOT:PSS Transparent Electrodes for Stretchable and Mechanically-Robust Organic Solar Cells. *Sol. Energy Mater. Sol. Cells* **2013**, *110*, 98–106.

(35) Pham, V. H.; Cuong, T. V.; Hur, S. H.; Shin, E. W.; Kim, J. S.; Chung, J. S.; Kim, E. J. Fast and Simple Fabrication of a Large Transparent Chemically-Converted Graphene Film by Spray-Coating. *Carbon* **2010**, *48*, 1945–1951.

(36) Hansbo, A.; Nylen, P. Models for the Simulation of Spray Deposition and Robot Motion Optimization in Thermal Spraying of Rotating Objects. *Surf. Coat. Technol.* **1999**, *122*, 191–201.

(37) Puetz, J.; Gasparro, G.; Aegeerter, M. A. Liquid Film Spray Deposition of Transparent Conducting Oxide Coatings. *Thin Solid Films* **2003**, *442*, 40–43.

(38) Bose, S.; Keller, S. S.; Alstrom, T. S.; Boisen, A.; Almdal, K. Process Optimization of Ultrasonic Spray Coating of Polymer Films. *Langmuir* **2013**, *29*, 6911–6919.

(39) Assad, O.; Leshansky, A. M.; Wang, B.; Stelzner, T.; Christiansen, S.; Haick, H. Spray-Coating Route for Highly Aligned and Large-Scale Arrays of Nanowires. *ACS Nano* **2012**, *6*, 4702–4712.

(40) Li, J. C.; Gong, X.; Wang, D.; Ba, D. C. Electrical Switching of Molecular Thin Films Filled in Metal Oxide Cracks. *Appl. Phys. A: Mater. Sci. Process.* **2013**, *111*, 645–651.

(41) Singh, K. B.; Tirumkudulu, M. S. Cracking in Drying Colloidal Films. *Phys. Rev. Lett.* **2007**, *98*, 218302.

(42) Lee, W. P.; Routh, A. F. Why Do Drying Films Crack? *Langmuir* **2004**, *20*, 9885–9888.

(43) Sorel, S.; Bellet, D.; Coleman, J. N. Relationship Between Material Properties and Transparent Heater Performance for both Bulk-like and Percolative Nanostructured Networks. *ACS Nano* **2014**, *8*, 4805–4814.

(44) De, S.; Coleman, J. N. The Effects of Percolation in Nanostructured Transparent Conductors. *MRS Bull.* **2011**, *36*, 774–781.

(45) Kang, T. J.; Kim, T.; Seo, S. M.; Park, Y. J.; Kim, Y. H. Thickness-Dependent Thermal Resistance of a Transparent Glass Heater with a Single-Walled Carbon Nanotube Coating. *Carbon* **2011**, *49*, 1087–1093.

(46) Lowell, E. B.; Holland, M. Process for Making a Curved, Conductively Coated Glass Member and the Product Thereof. U.S. Patent 4650557 A, 1984.

(47) Wu, H.; Kong, D.; Ruan, Z.; Hsu, P. C.; Wang, S.; Yu, Z.; Carney, T. J.; Hu, L.; Fan, S.; Cui, Y. A Transparent Electrode Based on a Metal Nanotrough Network. *Nat. Nanotechnol.* **2013**, *8*, 421–425.

(48) Siwei, Z.; Yuan, G.; Bin, H.; Jia, L.; Jun, S.; Zhiyong, F.; Jun, Z. Transferable Self-Welding Silver Nanowire Network as High Performance Transparent Flexible Electrode. *Nanotechnology* **2013**, *24*, 335202.